Rapid gravity flow transformation revealed in a single climbing ripple

Baas, Jaco H.; Best, Jim; Peakall, Jeff

Geology

DOI:
https://doi.org/10.1130/G48181.1

Published: 01/05/2021

Peer reviewed version

Rapid gravity flow transformation revealed in a single climbing ripple

Jaco H. Baas[1], Jim Best[2] and Jeff Peakall[3]

[1]School of Ocean Sciences, Bangor University, Menai Bridge LL59 5AB, UK, e-mail: j.baas@bangor.ac.uk

[2]Departments of Geology, Geography and GIS, Mechanical Science and Engineering, and Ven Te Chow Hydrosystems Laboratory, University of Illinois at Urbana-Champaign, Urbana, IL 61801, USA

[3]School of Earth and Environment, University of Leeds, Leeds, LS2 9JT, UK

ABSTRACT

Sediment gravity flows possess a wide range of rheological behaviors and past work has shown how transformations between flow types generate spatiotemporal changes in the resultant sedimentary successions. Herein, the geometrical characteristics of a single climbing ripple are used to demonstrate how such flows can transform from a turbulent to a quasi-laminar plug flow, with the transitional clay flow sequence being manifested by abnormally large heterolithic sand–clay current ripples with small backflow ripples, and then abundant clay deposition associated with smaller ripples. Analysis of ripple size, angle of climb, grain size, internal erosional surfaces and soft-sediment deformation suggest that transformation in the rheological character of the sediment gravity flow was rapid, occurring over a period of tens of minutes, and thus probably over a spatial scale of hundreds of meters to several kilometers. The present study indicates how the character of flow transformation can be elucidated from the details of a small-scale sedimentary structure.

INTRODUCTION

Sediment gravity flows (SGFs) in oceans and lakes are a vital component of the global sediment cycle (Hessler and Fildani, 2019), and are equally important for the transport of organic carbon, nutrients and pollutants (e.g., plastics; Kane et al., 2020), pose a hazard to infrastructure (Clare et al., 2019), and their deposits may store hydrocarbons (Talling, 2014). The research and socio-economic relevance of SGFs is widely appreciated, but studying SGFs is challenging because of their unsteady

and non-uniform behavior. This is exacerbated by the fact that most SGFs carry clay particles that aggregate to form floccules and gels, and thus enhance or suppress the shear-generated turbulence that helps drive these flows and shape their deposits (Baas et al., 2009; Baker et al., 2017). Detailed studies of SGF deposits have shown that these complex kinematics are expressed in the ability of SGFs to transform between turbulent, transitional and laminar behavior (Haughton et al., 2009), on which the concentration of suspended clay has a key influence (Baas et al., 2011). As clay concentration increases, these flow types comprise: (a) turbulence-enhanced transitional flow (TETF), in which turbulence is enhanced relative to clay-free turbulent flow; (b) lower transitional plug flow (LTPF), in which near-bed enhanced turbulence exists below a moving plug with suppressed turbulence; (c) upper transitional plug flow (UTPF), which has a thickened plug flow zone above a thinned, near-bed, zone of attenuated turbulence; and (d) quasi-laminar plug flow (QLPF), in which the plug extends down to the bed and turbulence is weak to absent (Baas et al., 2009). The characteristic bedforms formed by transitional flow are large ripples in TETF and LTPF and low-amplitude bed-waves in UTPF and QLPF (Baas et al., 2016). Large ripples have greater heights and wavelengths than ripples formed in clearwater, and low-amplitude bed waves are significantly longer and flatter than ripples generated in turbulent flows (Baker and Baas, 2020). Herein, we provide evidence for progressive SGF transformation preserved in a single climbing ripple, which stores a continuous record of bed aggradation and bedform migration. Since climbing ripples can form rapidly, especially at steep angles of climb associated with rapid aggradation rates (Allen, 1963), our analysis implies that flow transformation can occur in several tens of minutes. This timescale may be typical of transforming SGFs in confined basins (e.g., Fonnesu et al., 2015), but it is considerably shorter than for SGFs transforming in unconfined basins, which are usually 10s to 100s of km long and last for several hours to days or even weeks (Azpiroz-Zabala et al., 2017).

MATERIAL AND METHODS

We investigated a climbing-ripple set in a polished slab from the Seathwaite Fell Sandstone Formation (Ordovician, Elterwater Quarry, UK, 54.435°N, 3.046°W). This set forms a representative part of a climbing ripple co-set with similar sedimentological properties (Fig. 1A; Supplementary Material; Fig. S1), formed by deposition from a volcaniclastic mixed sand–clay gravity flow in a caldera lake (Branney and Kokelaar, 1994). The Seathwaite Fell Sandstone Formation contains various other types of primary current lamination, and soft-sediment deformation structures, denoting high sediment accumulation rates and seismic instability (Barnes et al., 2006).

The climbing-ripple set was divided into three sectors, based on textural properties, and 21 ripple positions were defined in these sectors by tracing ripple outlines (Fig. 1B). These positions were then used to determine the evolution of ripple height (Fig. 1C; the vertical distance between ripple trough

and crest), and, where possible, ripple wavelength (the horizontal distance between adjacent ripple troughs). Ripple brinkpoints were traced to determine changes in angle of climb, and the size of sand grains was measured using a Dino-Lite digital microscope. Ripple types were then interpreted, based on ripple size and their turbulent, transitional and laminar flow signatures (Baas et al., 2009, 2011, 2016). Finally, qualitative evidence for rapid bed aggradation was combined with quantitative analysis using several methods (Fig. 1D) that have been proposed previously (Supplementary Material; Ashley et al., 1982; Baas, 1993, 2004; Baas et al., 2000, 2009; Jobe et al., 2012) to determine bed aggradation rates (Supplementary Material) and estimate the duration of deposition of the climbing-ripple set.

THE CLIMBING-RIPPLE SET EXPLAINED KINEMATICALLY

Description: In Sector 1 (yellow lines, Fig. 1B), the ripple is sandy and climbs over a vertical distance of 15.6 mm at a mean angle of 19.7°. Sector 2 is 27.7 mm thick, with a mean angle of climb of 18.4° (orange lines, Fig. 1B), and possesses distinct foreset laminae of alternating sand and clay. The mean sand size in Sectors 1 and 2 is 0.124 mm. Sector 3 (red lines, Fig. 1B) is clay-rich with occasional thin, discontinuous, silty laminae; the ripple climbs over a vertical distance of 21.6 mm at a mean angle of 44.2°. The ripple height in Sector 1 increases from 8.5 to 12.9 mm (Figs. 1C and 2), and keeps growing in Sector 2, until it reaches a maximum height of 21.7 mm at the transition to Sector 3 (Figs 1C and 2). In Sector 3, ripple height and wavelength decrease from 21.7 to 18.4 mm (Figs 1C and 2) and from 174 to 183 mm (Fig. 1B), respectively.

Interpretation: The final ripple height of 12.9 mm in Sector 1 is less than 14.9 mm, the height at which equilibrium ripples form in 0.124 mm sand under clearwater flow (Baas, 1993; Fig. 2). It is therefore inferred that this ripple did not reach equilibrium and evolved between non-equilibrium heights of 8.5 and 12.9 mm. The sandy nature of Sector 1 suggests that any suspended clay present did not affect the flow kinematics or become incorporated into the bed. Hence, this ripple formed in a ‘classic’ fully turbulent flow (Baas et al., 2011; Fig. 3B). The ripple grew in height throughout Sector 2 (Figs. 2 and 3C), with the final height of 21.7 mm matching the so-called ‘large ripples’ generated in the laboratory (Baas et al., 2016) and described in outcrop (Baker and Baas, 2020; Fig. 2). Large ripples form in TETF and LTPF (Baas et al., 2011; Fig. 3C), in which enhanced turbulence in ripple troughs (Baas and Best, 2008) helps to increase ripple size. This turbulence enhancement requires a local increase in suspended clay concentration, possibly combined with flow deceleration (Figs 3C and S2). Further support for TETF and LTPF comes from: (a) alternating sandy and clayey laminae in Sector 2, which mimics large ripples in the laboratory (Baas et al., 2011, 2016); (b) small backflow ripples near the base of the ripple foreset (Fig. S3), pointing to strong vorticity and upstream flow velocities in the ripple trough (Baas et al., 2011); and (c) a finer-grained core (sensu Baker and Baas,

2020), especially in the top half of Sector 2 (Fig. 1A), across which the sandy part of the ripple migrated, signifying concurrent bedload transport of sand and fallout from suspension of clay. The ripple in Sector 3 has a smaller height than in Sector 2 (Fig. 2), interpreted as the product of a further increase in local suspended clay concentration combined with flow deceleration in an UTPF or QLPF (Supplementary Material) that caused the ripple height to decrease (Fig. 3D). This is supported by the high clay content in Sector 3, denoting significant fallout from suspension, and the fact that Baker and Baas (2020) have shown that such flows form low-amplitude bed-waves, the height of which is much smaller (mostly below 10 mm) and the wavelength of which is larger (200-800 mm) than for ripples in turbulent and turbulence-enhanced flows. However, the bedform in Sector 3 did not reach these heights and wavelengths (Fig. 2), probably because ripple development was temporarily constrained and the high suspended clay concentration hindered evolution from large ripples to low-amplitude bed-waves. These bedforms can therefore be classified as relict large ripples.

The ripple studied herein climbed at high mean angles of 18.4° to 44.2°, suggesting that the vertical aggradation rate became larger relative to the migration rate (Supplementary Material). Various quantitative methods (Fig. 1D; see Supplementary Material for details) show that a period of the order of tens of minutes, with extremes in the Sectors 1 to 3 of 1.2-38.8 minutes, 5.9-125 minutes, and 8.2-69 minutes, respectively, was sufficient to deposit the climbing-ripple set. Such rapid development is also supported by qualitative data (Fig. 1A): (a) Strong erosion (>10 mm deep, Figs 1A and 3A) and soft-sediment deformation of clay-rich sediment at the base of the climbing-ripple co-set indicate that the initial flow conditions were strong enough to deform and erode cohesive clay. The occasional presence of mud clasts confirms that the substrate was firm. (b) Flow in the ripple trough was fast enough to scour into the stoss side of the downstream ripple in Sectors 1 and 2 (Fig. 1A). (c) soft-sediment deformation in Sector 3 (Fig. 1A) may indicate water-rich sediment linked to rapid deposition (Barnes et al., 2006). This deformation was synsedimentary because local deformation is healed by younger laminae.

FLOW TRANSFORMATION IN CLIMBING RIPPLES: IMPLICATIONS

The present study reveals that climbing ripples can preserve continuous records of transformation from turbulent via transitional to laminar flow in a waning, mixed sand–clay, gravity current (Fig. 3), and it confirms that kinematic process models for ripples in sand do not apply to ripples in mixed sand–clay (Baas et al., 2016; Baker and Baas, 2020). This is not unique to the Seathwaite Fell Sandstone Formation. Climbing-ripple co-sets with an upward increase in angle of climb, and wavelength, are one of three climbing ripple patterns in the classification of Allen (1973), and have been linked to ‘collapsing flows’ in SGFs (Jobe et al., 2012), implying that suspension fallout rates increased during deposition relative to bedload transport rate. However, this does not explain the

simultaneous increase in ripple wavelength. We infer that the steep angle of climb near the top of co-sets is caused not only by a strong increase in suspension fallout rate (e.g., Sorby, 1908; Allen, 1963; Hunter, 1977) and a decrease in ripple migration rate at decreased flow velocity (cf., Jopling and Walker, 1968), but also by a slowing of ripple migration through turbulence attenuation induced by cohesive clay (Baas et al., 2011). The mud-rich, longer-wavelength bedforms similar to those in Sector 3, found at the top of these sequences (Walker, 1963; Jopling and Walker, 1968; Bhattacherjee, 1970) also reflect flow transformation. For example, Bhattacherjee (1970) described muddy bedforms in the Cloridorme Formation (Québec, Canada), 13.6 mm high and 353 mm long, which match the size of low-amplitude bed-waves (Baas et al., 2016; Baker and Baas, 2020; Fig. 2). Bhattacherjee (1970) also described ripples with a similar wavelength but a larger height (27 mm; his figure 8) in clay-rich sandstones below climbing low-amplitude bed-waves, thus resembling large ripples (Baas et al., 2016; Baker and Baas, 2020; cf., Stanley, 1974; Fig. 2). This change from large ripples to low-amplitude bed-waves matches the climbing-ripple co-set studied herein, except that the bedforms in the Cloridorme Formation were able to fully complete this change.

It thus appears that the climbing ripples described herein are a common sedimentary structure. They resemble the Type-3 climbing ripple co-sets of Walker (1963; his table II), almost exclusively found in turbidites. Therefore, in addition to providing evidence for flow transformation, the mixed sand–clay climbing ripple co-sets described herein may also be a strong indicator for waning gravity flows in deep-marine or lacustrine depositional environments. In most scenarios, waning mixed sand–clay gravity flows must pass through flow types in which turbulence is first enhanced and then attenuated (Fig. S1), and thus large ripples and low-amplitude bed-waves can be expected to be common bedform types in mixed sand–clay climbing ripple co-sets. Together with sandy ripples, these bedforms provide a novel tool to reconstruct temporal changes in SGF kinematics.

The present analysis illustrates that rates of flow transformation in SGFs, and thus rates at which cohesivity may develop, can be as rapid as several tens of minutes. In the example described herein, this duration converts into flow lengths of hundreds of meters to several kilometers for flow velocities at which current ripples are stable. These temporal and spatial scales correspond to those inferred from the deposits of SGFs that comprise a hybrid between turbulent and laminar behavior in confined basins (e.g., Fonnesu et al., 2015). However, these scales are at least an order of magnitude shorter than for unconfined basins, which usually contain rapid flows that are 10s to 100s of km long (e.g., Haughton et al., 2009; Talling, 2013; Talling et al., 2013) and may last for several hours to days or even weeks (Azpiroz-Zabala et al., 2017). The present analysis shows that once such flows start to decelerate, transformation can occur rapidly, and that SGF deposits can leave evidence of this flow transformation at a scale of 10s of mm that can be recognized in cores and small outcrops.

CONCLUSIONS

The rate of flow transformation within a SGF is revealed by analysis of bedform size, grain size and the microstructure of cross-stratification within a single climbing ripple set. The present study demonstrates that an initially turbulent flow that is aggradational and generates climbing ripples, begins to develop large ripples in TETF or LTPF, as the flow decelerates. These large ripples are generated by increased turbulence in the ripple trough that causes additional scour that may also form small backflow ripples. These large ripples are also characterized by heterolithic deposition on the ripple leeside, as fallout from suspension becomes more dominant than sand and silt avalanching down the leeside slope. Further flow deceleration, and increases in clay concentration, cause more rapid aggradation, and higher angles of climb, of the clay-rich current ripple, which also becomes smaller due to the dampening of turbulence in UTPF or QLPF. Further analysis reveals that such flow transformation, from turbulent to quasi-laminar plug flow, was rapid and occurred over a period of tens of minutes, suggesting that the spatial distance over which such transformation took place was hundreds of meters to several kilometers. Quantification of the microstructure of such climbing ripple sequences may hold untapped potential for reconstructing the temporal fluid dynamics of clay-laden SGFs in many sedimentary environments.

ACKNOWLEDGMENTS

We thank Fiona Cameron, Burlington Stone, UK, for arranging access to these materials, and Zane Jobe, Matthieu Cartigny, and Bill Arnott for their insightful reviews.

REFERENCES CITED

Allen, J. R. L., 1963, Asymmetrical ripple marks and the origin of water-laid cosets of cross-strata: Liverpool Manchester Geological Journal, v. 3, p. 187-236.

Allen, J. R. L., 1973, A classification of climbing-ripple cross-lamination: Journal of the Geological Society of London, v. 129, p. 537-541.

Ashley, G. M., Southard, J. B., and Boothroyd, J. C., 1982, Deposition of climbing-ripple beds: a flume simulation: Sedimentology, v. 29, p. 67-79.

Azpiroz-Zabala, M., Cartigny, M. J. B., Talling, P. J., Parsons, D. R., Sumner, E. J., Clare, M. A., Simmons, S. M., Cooper, C., and Pope, E. L., 2017, Newly recognized turbidity current structure can explain prolonged flushing of submarine canyons: Science Advances, v. 3, e1700200.

Baas, J. H., 1993, Dimensional analysis of current ripples in recent and ancient depositional environments: Geologica Ultraiectina, v. 106, p. 199.

Baas, J. H., 2004, Conditions for formation of massive turbiditic sandstones by primary depositional processes: Sedimentary Geology, v. 166, p. 293-310.

Baas, J. H., and Best, J. L., 2008, The dynamics of turbulent, transitional and laminar clay-laden flow over a fixed current ripple: Sedimentology, v. 55, p. 635-666.

Baas, J. H., Best, J. L., Peakall, J., and Wang, M., 2009, A phase diagram for turbulent, transitional, and laminar clay suspension flows: Journal of Sedimentary Research, v. 79, p. 162-183.

Baas, J. H., Best, J. L., and Peakall, J., 2011, Depositional processes, bedform development and hybrid flows in rapidly decelerated cohesive (mud-sand) sediment flows: Sedimentology, v. 58, p. 1953-1987.

Baas, J. H., Best, J. L., and Peakall, J., 2016, Predicting bedforms and primary current stratification in cohesive mixtures of mud and sand: Journal of the Geological Society, v. 173, p. 12-45.

Baas, J. H., van Dam, R. L., and Storms, J. E. A., 2000, Duration of deposition from decelerating high-density turbidity currents: Sedimentary Geology, v. 136, p. 71-88.

Baker, M. L., and Baas, J.H., 2020, Mixed sand–mud bedforms produced by transient turbulent flows in the fringe of submarine fans: Indicators of flow transformation: Sedimentology, v. 67, p. 2645-2671.

Baker, M. L., Baas, J. H., Malarkey, J., Silva Jacinto, R., Craig, M. J., Kane, I. A., and Barker, S., 2017, The effect of clay type on the properties of cohesive sediment gravity flows and their deposits: Journal of Sedimentary Research, v. 87, p. 1176-1195.

Barnes, R. P., Branney, M. J., Stone, P., and Woodcock, N.H., 2006, The Lakesman Terrane: the Lower Palaeozoic record of the deep marine Lakesman Basin, a volcanic arc and foreland basin, *in* Brenchley, P.J., and Rawson, P.F., eds., The Geology of England and Wales, Geological Society, London, Geology Of Series, p. 103-130.

Bhattacharjee, S. B., 1970, Ripple-drift cross-lamination in turbidites of the Ordovician Cloridorme Formation, Gaspé, Québec [M.Sc. Thesis], McMaster University, Hamilton, Ontario, Canada, 281 p.

Branney, M. J., and Kokelaar, P., 1994, Volcanotectonic faulting, soft-state deformation, and rheomorphism of tuffs during development of a piecemeal caldera, English Lake District: Geological Society of America Bulletin, v. 106, p. 507-530.

Clare, M., Chaytor, J., Dabson, O., Gamboa, D., Georgiopoulou, A., Eady, H., Hunt, J., Jackson, C., Katz, O., Krastel, S., León, R., Micallef, A., Moernaut, J., Moriconi, R., Moscardelli, L., Mueller, C., Normandeau, A., Patacci, M., Steventon, M., Urlaub, M., Völker, D., Wood, L., and Jobe, Z., 2019, A consistent global approach for the morphometric characterization of subaqueous landslides: Geological Society, London, Special Publications, v. 477, p. 455-477.

Fonnesu, M., Haughton, P., Felletti, F., and McCaffrey, W., 2015, Short length-scale variability of hybrid event beds and its applied significance: Marine and Petroleum Geology, v. 67, p. 583-603.

Haughton, P., Davis, C., McCaffrey, W., and Barker, S., 2009, Hybrid sediment gravity flow deposits - Classification, origin and significance: Marine and Petroleum Geology, v. 26, p. 1900-1918.

Hessler, A.M., and Fildani, A., 2019, Deep-sea fans: Tapping into Earth's changing landscapes: Journal of Sedimentary Research, v. 89, p. 1171-1179.

Hunter, R.E., 1977, Terminology of cross-stratified sedimentary layers and climbing-ripple structures: Journal of Sedimentary Petrology, v. 47, p. 697-706.

Jobe, Z. R., Lowe, D. R., and Morris, W. R., 2012, Climbing-ripple successions in turbidite systems: depositional environments, sedimentation rates and accumulation times: Sedimentology, v. 59, p. 867-898.

Jopling, A. V., and Walker, R. G., 1968, Morphology and origin of ripple-drift cross-lamination, with examples from the Pleistocene of Massachusetts: Journal of Sedimentary Petrology, v. 38, p. 971-984.

Kane, I. A., Clare, M. A., Miramontes, E., Wogelius, R., Rothwell, J.J., Garreau, P., and Pohl, F., 2020, Seafloor microplastic hotspots controlled by deep-sea circulation: Science, v. 368, p. 1140-1145.

Sorby, H. C., 1908, On the application of quantitative methods to the study of the structure and history of rocks: Quarterly Journal of the Geological Society of London, v. 64, p. 171-233.

Stanley, K. O., 1974, Morphology and hydraulic significance of climbing ripples with superimposed micro-ripple-drift cross-lamination in lower Quaternary lake silts, Nebraska: Journal of Sedimentary Petrology, v. 44, p. 472-483.

Talling, P. J., 2013, Hybrid submarine flows comprising turbidity current and cohesive debris flow: Deposits, theoretical and experimental analyses, and generalized models: Geosphere, v. 9, p. 460-488.

Talling, P. J., 2014, On the triggers, resulting flow types and frequencies of subaqueous sediment density flows in different settings: Marine Geology, v. 352, p. 155-182.

Talling, P. J., Paull, C. K., and Piper, D. J. W., 2013, How are subaqueous sediment density flows triggered, what is their internal structure and how does it evolve? Direct observations from monitoring of active flows: Earth-Science Reviews, v. 125, p. 244-287.

Walker, R. G., 1963, Distinctive types of ripple-drift cross-lamination: Sedimentology, v. 2, p. 173-188.

FIGURE CAPTIONS

Figure 1. (A) Climbing-ripple co-set in Seathwaite Fell Sandstone Formation, UK. Inset shows location of (B). Flow direction is towards right. (B) High-contrast image of the climbing-ripple set, highlighting 21 ripple outlines in Sectors 1 (yellow), 2 (orange), and 3 (red). Blue dashed line traces the ripple brinkpoints. Inset shows location of Fig. S3. TF = turbulent flow; TETF = turbulence-enhanced transitional plug flow; LTPF/UTPF = lower/upper transitional plug flow; QLPF = quasi-laminar plug flow. (C) Horizontal position of the ripple brinkpoint vs ripple height and angle of climb for the three sectors. Numbers refer to ripple outlines in (B). (D) Estimated durations of deposition of Sectors 1 (yellow), 2 (orange), and 3 (red), using the methods described in the Supplementary Material. Note that the range for bed sediment flux & ripple height in Sector 2 may be overestimated (see Supplementary Material).

Figure 2. Compilation of wavelengths and heights for sandy ripples, large ripples and low-amplitude bed-waves. Black box: predicted size range of non-equilibrium and equilibrium ripples in 0.124 mm sand (Baas, 1993). Yellow dots: sandy ripples for a range of grain sizes. Note that all large ripples and low-amplitude bed-waves are outside the size range of ripples in 0.124 mm sand.

Figure 3. Schematic model for the formation of the climbing-ripple set. (A) Erosion by turbulent flow front. (B) Sandy ripples formed by turbulent body of flow. (C) Mixed sand–clay large ripples formed by turbulence-enhanced flow. (D) Clay-rich ripples formed by turbulence-attenuated flow. (E) Schematic temporal changes in flow velocity, near-bed clay concentration and turbulence, sand and clay aggradation rate, and angle of climb. See Fig. 1 for explanation of flow types.

Figure 1

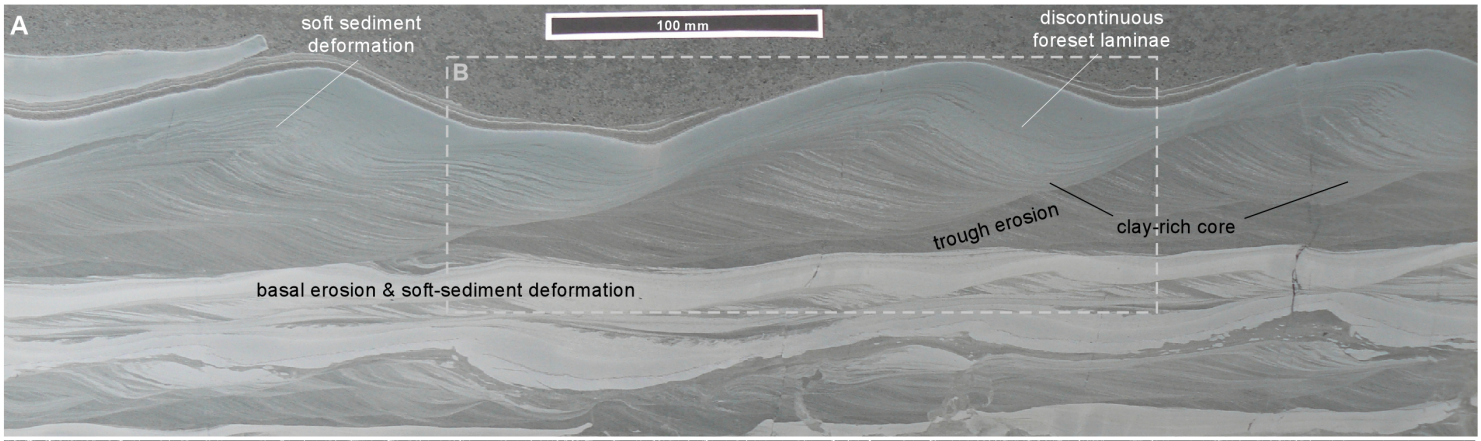
A
soft sediment deformation
100 mm
B
discontinuous foreset laminae
trough erosion
clay-rich core
basal erosion & soft-sediment deformation

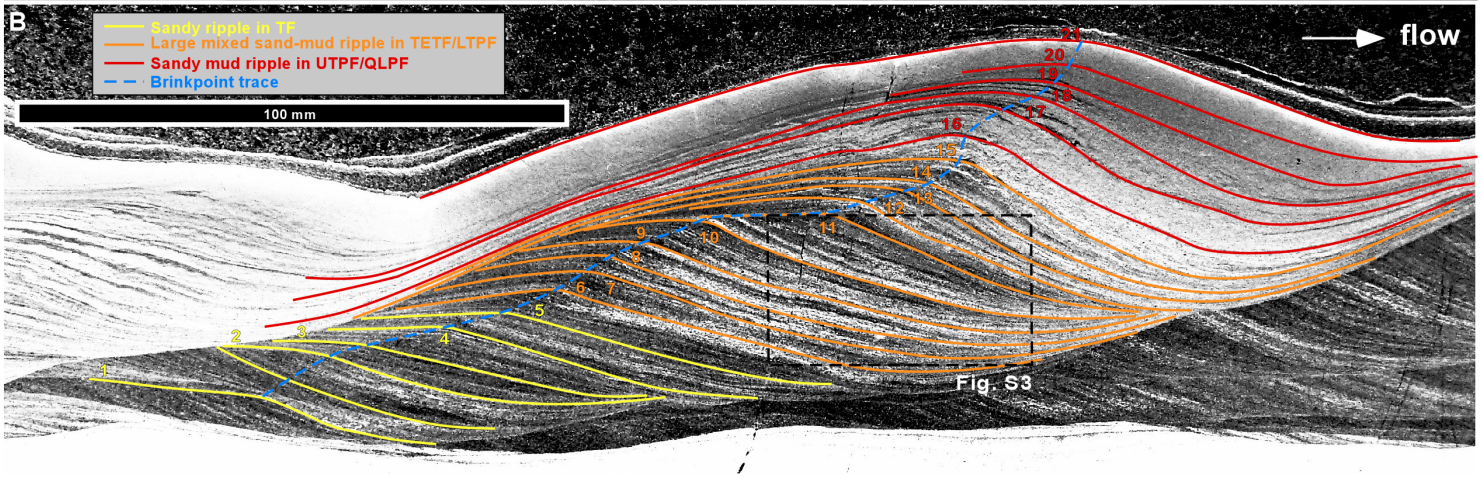
B
Sandy ripple in TF
Large mixed sand-mud ripple in TETF/LTPF
Sandy mud ripple in UTPF/QLPF
Brinkpoint trace
100 mm
flow
Fig. S3

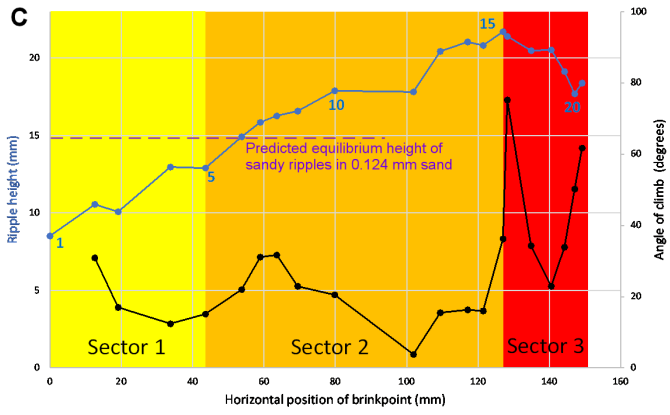
C
Ripple height (mm)
Angle of climb (degrees)
Predicted equilibrium height of sandy ripples in 0.124 mm sand
Sector 1
Sector 2
Sector 3
Horizontal position of brinkpoint (mm)

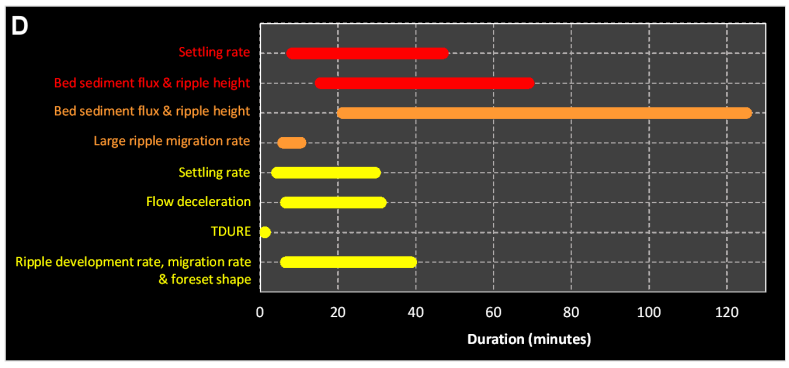
D
Settling rate
Bed sediment flux & ripple height
Bed sediment flux & ripple height
Large ripple migration rate
Settling rate
Flow deceleration
TDURE
Ripple development rate, migration rate & foreset shape
Duration (minutes)

Figure 2

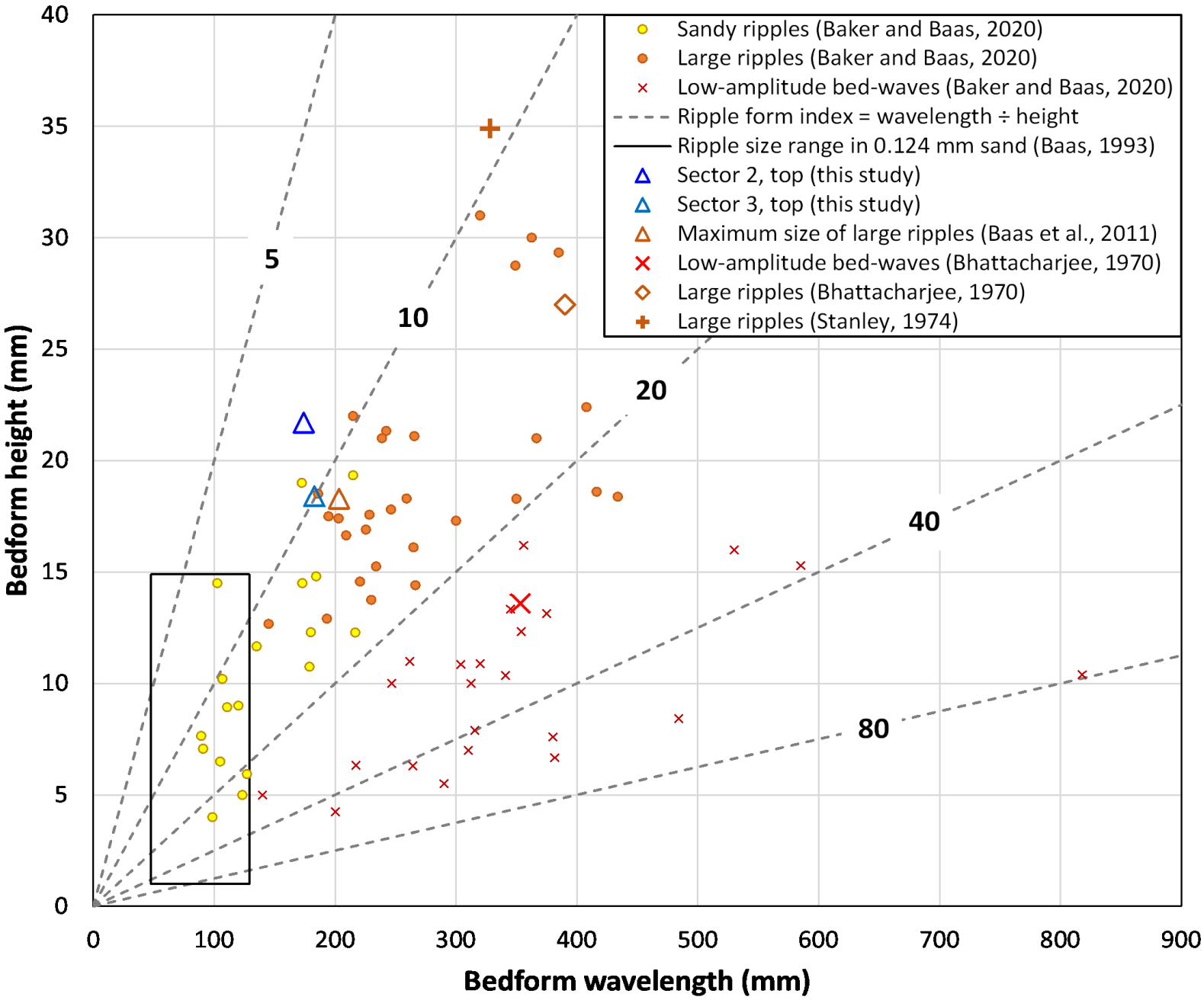
Sandy ripples (Baker and Baas, 2020)
Large ripples (Baker and Baas, 2020)
Low-amplitude bed-waves (Baker and Baas, 2020)
Ripple form index = wavelength ÷ height
Ripple size range in 0.124 mm sand (Baas, 1993)
Sector 2, top (this study)
Sector 3, top (this study)
Maximum size of large ripples (Baas et al., 2011)
Low-amplitude bed-waves (Bhattacharjee, 1970)
Large ripples (Bhattacharjee, 1970)
Large ripples (Stanley, 1974)
5
10
20
40
80
Bedform height (mm)
Bedform wavelength (mm)
0
5
10
15
20
25
30
35
40
0
100
200
300
400
500
600
700
800
900

Figure 3

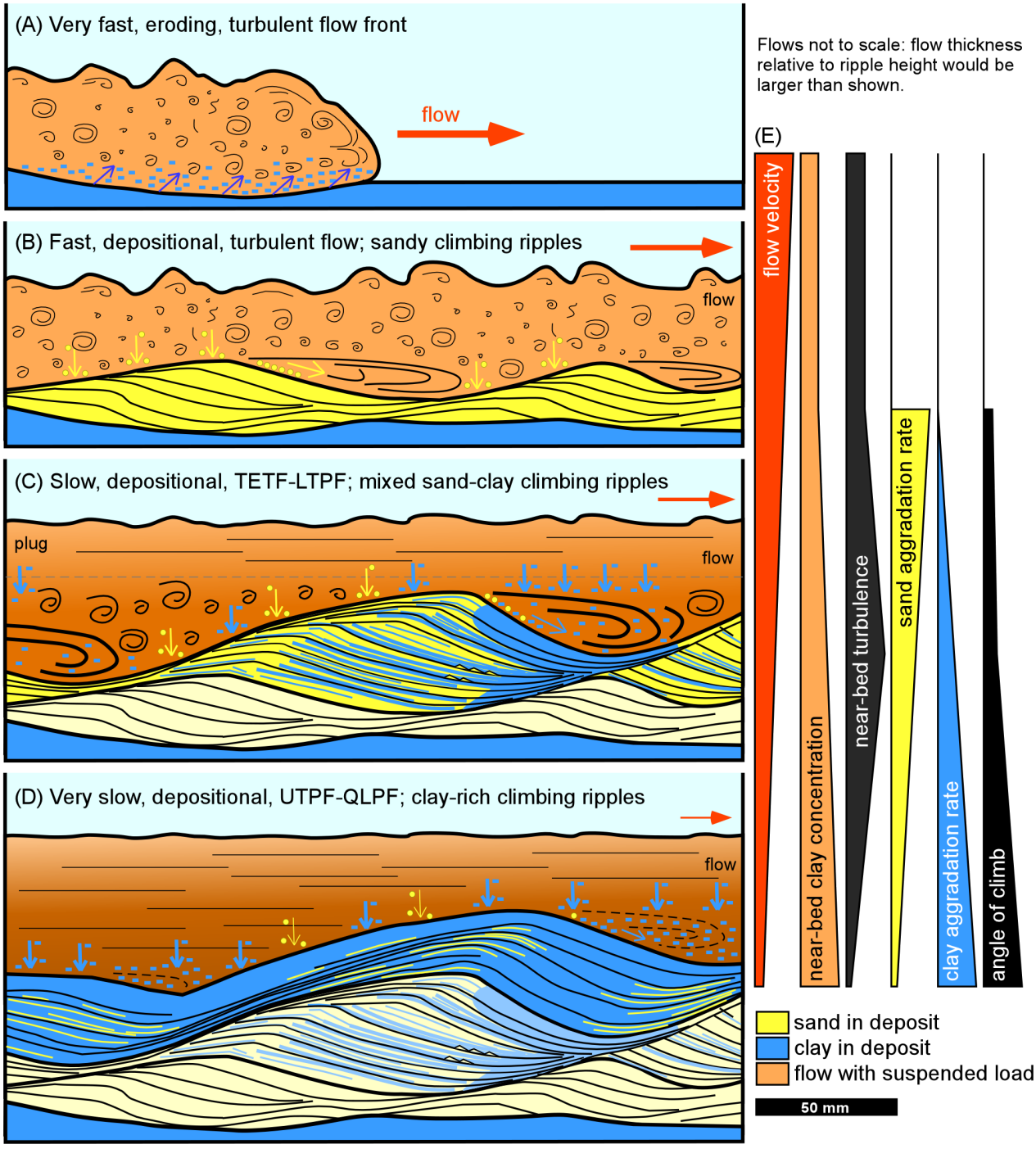
(A) Very fast, eroding, turbulent flow front
flow
(B) Fast, depositional, turbulent flow; sandy climbing ripples
flow
(C) Slow, depositional, TETF-LTPF; mixed sand-clay climbing ripples
plug
flow
(D) Very slow, depositional, UTPF-QLPF; clay-rich climbing ripples
flow
Flows not to scale: flow thickness relative to ripple height would be larger than shown.
(E)
flow velocity
near-bed clay concentration
near-bed turbulence
sand aggradation rate
clay aggradation rate
angle of climb
sand in deposit
clay in deposit
flow with suspended load
50 mm